Science of the Total Environment 654 (2019) 1118–1131

Contents lists available at ScienceDirect

Science of the Total Environment

journal homepage: www.elsevier.com/locate/scitotenv

The effect of brine pumping on the natural hydrodynamics of the Salar de Atacama: The damping capacity of salt flats

M.A. Marazuela [a,b,c,*], E. Vázquez-Suñé [a], C. Ayora [a], A. García-Gil [d], T. Palma [a]

[a] Institute of Environmental Assessment and Water Research (IDAEA), CSIC, Jordi Girona 18-26, 08034 Barcelona, Spain
[b] Department of Civil and Environmental Engineering, Technical University of Catalonia (UPC), Jordi Girona 1-3, 08034 Barcelona, Spain
[c] Associated Unit: Hydrogeology Group (UPC-CSIC), Spain
[d] Geological and Mining Institute of Spain (IGME), Manuel Lasala 44, 9° B, 50006 Zaragoza, Spain

HIGHLIGHTS

- 3D groundwater flow modelling of the Salar de Atacama
- Damping capacity of salt flats water table was defined.
- Brine pumping causes reduction in the evaporation rate of salt flats.
- Reduction of evaporation due to brine pumping damping the water table drawdown
- The damping capacity ends up when the water table is depleted below 0.5–2 m deep.

GRAPHICAL ABSTRACT

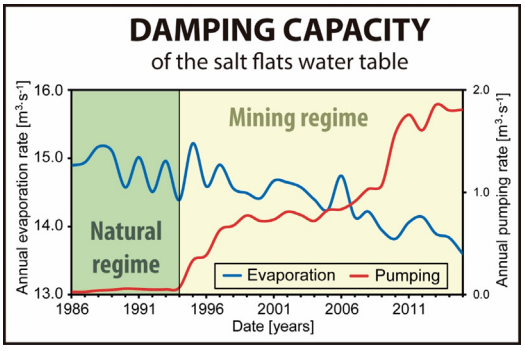

ARTICLE INFO

Article history:
Received 22 December 2017
Received in revised form 13 November 2018
Accepted 13 November 2018
Available online 14 November 2018

Editor: Damia Barcelo

Keywords:
Groundwater management
Numerical modelling
Evaporation
Brine
Pumping
Lithium

ABSTRACT

The Salar de Atacama is used as a case study to analyse and quantify coupled natural (evaporation and recharge) and anthropogenic processes (pumping of lithium-rich brine) to abstract their patterns to other salt flats using a three-dimensional groundwater flow model. Important changes in the dynamics of the water table between the pre-operational period (1986–1994) and operational period (1994–2015) are observed. The water table exhibited a gradual drawdown during the pre-operational period because the evaporation was greater than the recharge for most of these periods. This negative balance was counteracted by some sharp rises that were produced by direct rainfall events on the salt flat. The deep lateral recharge that arrived from the mountains did not produce abrupt changes in the water table because the rainfall events in the mountains were damped by the distance of the recharge zone and great thickness of the unsaturated zone.

The natural evolution of the water table was modified by the intensive brine pumping that was performed in the south-western Salar de Atacama during the operational period. As evaporation depends on the water table depth, the pumping caused a drawdown of the water table, resulting in an evaporation rate reduction that partially compensated for the pumped brine in the water balance of the basin. This effect is defined as the *damping capacity* of salt flats. Thus, salt flats have a high capacity for dampening oscillations in their water table in response to both natural and anthropogenic disturbances which is of great importance for the management of lake and wetland ecosystems and brine exploitation. The limit of the dampening capacity of salt flats is defined by the evaporation extinction depth, which is in the range of 0.5–2 m.

* Corresponding author at: Institute of Environmental Assessment and Water Research (IDAEA), CSIC, Jordi Girona 18, 08034 Barcelona, Spain.
E-mail address: mamarazuela@outlook.com (M.A. Marazuela).

https://doi.org/10.1016/j.scitotenv.2018.11.196
0048-9697/

1. Introduction

The Salar de Atacama is the largest source of lithium in the world, containing approximately a quarter part of the global reserves. It is, behind the Salar de Uyuni (Bolivia) and Salinas Grandes (Argentina), the third largest salt flat of the Altiplano and of the world (Risacher et al., 2003). Brine of salt flats is also a source of large amounts of boron, potassium, iodine, sodium chloride and bischofite (Evans, 1978; Hardie, 1991; Kesler et al., 2012; Lowenstein and Risacher, 2009; Munk et al., 2016; Rissmann et al., 2015). These elements and minerals are essential for the production of batteries, fertilizers, ceramics, detergents and other important industrial utilities (Marom et al., 2011; Vikström et al., 2013). The exploitation of lithium and other chemical elements is executed through brine pumping. The extracted brine is channelled into large pools where it evaporates and precipitates salts, returning a part of the excess brine to the aquifer via infiltration or reinjection wells. The boom in clean energy production forecasts an increase in the demand for these elements and minerals that could trigger significant ecological impacts on salt flat ecosystems. Therefore, understanding the hydrodynamics of these hydrogeological systems is important for predicting their response to anthropogenic pressure and for proposing solutions for their sustainable management.

Salt flats are saline dry lakes often associated with arid to hyperarid environments in which the water table is located close to the land surface, allowing phreatic evaporation from groundwater. Under the natural regime, the depth of the water table is a result of the balance between the recharge produced mainly by rainfall in the mountains and the evaporation produced in the salt flat (Yechieli and Wood, 2002). The high evaporation rates maintained for thousand or millions of years allow the accumulation of large amounts of salts (Corenthal et al., 2016; Warren, 2010; Wood and Sanford, 1990).

As a consequence of the density contrast between the brine produced from evaporation and the freshwater recharged in the mountains, a saline interface with a mixing zone is often present in the margins of the salt flats (Fan et al., 1997; Hamann et al., 2015; Holzbecher, 2005; Nield et al., 2008; Wooding et al., 1997). When the groundwater recharged in the mountains arrives at the marginal zone of the salt flat, it is forced upward by its lower density. In the marginal zone where the mixing zone is located, many lakes and wetlands with valuable ecosystems exist, favoured by the upward groundwater flow. Moreover, in the salt flat, the evaporated brine sinks due to its high density, and when it arrives at the mixing zone, it can be forced to return to the land surface of the mixing zone by convection cells, causing mixing with the freshwater that comes from the mountains (Marazuela et al., 2018).

As the salt flats water table is controlled by evaporation and recharge processes, these systems are very sensitive to climatic and anthropogenic changes (Rosen, 1994). Climatic cycles may cause a direct response in hydraulic heads at different scales (Bowen et al., 2017; Duffy and Al-Hassan, 1988). Moreover, the anthropogenic pressure upstream of the salt flats or directly in the same salt flat can generate large disturbances to the water table (Acosta and Custodio, 2008; Tyler et al., 2006) and therefore in the ecosystems depending on it. The study of some of these processes that join in the hydrodynamics of salt flats has been addressed in a separate manner in previous studies. Such is the case for the evaporation and rainfall in the Altiplano. Evaporation occurs directly from the groundwater due to the shallow water table, which favours the rise of water by capillarity. The evaporation in salt flats can reach the potential evaporation rate in open water reservoirs, but this rate decreases exponentially until extinguishing in the range of 0.6–2 m of depth (Kampf et al., 2005; Kampf and Tyler, 2006; Muñoz-Pardo et al., 2004). This causes the fluctuations of the water table due to natural or anthropogenic processes to modify the evaporation rate. Rainfall in the Altiplano basins is conditioned by topography, which, due to the Altiplano uplift, results in two rainfall domains, one more arid at lower elevations and another wetter one at high elevations (Bookhagen and Strecker, 2008; Boutt et al., 2016; Houston, 2006; Rech et al., 2006). To the best of the authors' knowledge, there are no studies that integrate in a coupled manner all natural processes with the pumping of brine. Based on numerical models, Muñoz-Pardo et al. (2004) developed a direct relationship between the water table depth and recharge and evaporation and investigated how this relationship could contribute to keeping the water table stable, but a detailed study of this process and the effect of brine pumping is still lacking. Acosta and Custodio (2008) evaluated the environmental impacts under different pumping rates in the exploitation of the Salar de Huasco (Chile), although they could not compare with measured data for the case studied.

Numerical models are the best tool capable of integrating all components of the water balance to analyse its interactions and to quantify the effects that brine pumping has on the water table. No previous study has integrated all natural and anthropogenic processes at the same time to reproduce the water table evolution of a salt flat in a three-dimensional (3D) numerical model. Additionally, no study has analysed the response of salt flats to the intensive pumping of brine and how this affect the natural regime of the water table. The high computational cost and the difficulty of quantifying the water balance of these basins are the reasons why these systems have rarely been quantitatively modelled.

To fill this scientific gap, the Salar de Atacama is a suitable case study. The monitoring network of the Salar de Atacama is considered the largest in the world (Tyler et al., 2006), and it has hydraulic head and density data spanning >30 years. The range of the continuous data record covers a first period (1986–1994) in which the hydrodynamics of the system were dominated by natural processes (the pre-operational period in an almost-natural regime) and a second period (1994–2015), in which the effect of the intensive extraction of brine was added (the operational period in the mining or anthropogenic regime).

Marazuela et al. (2018) used the Salar de Atacama to describe the hydrodynamics of the mixing zone in salt flats and to propose a methodology of hydraulic head corrections based on density variations to approximate the vertical fluxes of the mixing zone in constant-density 3D numerical models at the regional scale. This allows overcoming the limitation of the high computational cost of 3D models with variable density. Furthermore, the 3D steady-state numerical model of Marazuela et al. (2019) established the average water balance and groundwater flow of the Salar de Atacama in its natural regime, which serve to evidence that the infiltration in hyperarid basins reaches values much higher than what was previously believed. In their work, the water balance of the Salar de Atacama basin was established to be 16 $m^3 \cdot s^{-1}$ for both the recharge and evaporation, allowing a 0 $m^3 \cdot s^{-1}$ net balance. However, the temporal evolution of the water table and the effect of the hydrodynamics of the natural processes coupled to the brine pumping were outside the scope of the research and have not yet been studied. Understanding how brine pumping has affected the natural hydrodynamics of the Salar de Atacama for more than three decades is of great importance to know how salt flats respond to anthropogenic pressure and how this may affects their ecosystems. This is of paramount importance because salt flats (and their ecosystems) are becoming increasingly targeted for mining raw material critical for modern industry.

The objective of this paper is to study the interaction between the natural and anthropogenic processes that coexist in salt flats, using the Salar de Atacama as a case study, and to abstract natural and anthropogenic patterns to other salt flats. For this purpose, a 3D transient-state numerical model is used as a tool to describe and quantify the water table response to these coupled processes.

2. Study area

The Salar de Atacama basin is located in a large endorheic basin of the current forearc of northern Chile. The surface area of the basin is

approximately 17,000 km^2, and its depocenter (2300 m a.s.l., meters above sea level) is the Salar de Atacama. It belongs to the Antofagasta Region, located 55 km south of San Pedro de Atacama and 320 km northeast of Antofagasta (Fig. 1). The basin may be divided into four geomorphological domains: salt flat nucleus, mixing zone, alluvial fans and basement and volcanic rocks.

The eastern limit of the basin is represented by the Western Cordillera, which is the current volcanic arc of the Andean Range and reaches 5000 m a.s.l. The western limit of the basin is the Cordillera Domeyko, which has an average elevation of 3000 m a.s.l. and is constituted by Paleozoic and Mesozoic rocks (Arriagada et al., 2006; Pananont et al., 2004). At its southern boundary, the basin is limited by the Cordón de Lila, which includes igneous and sedimentary rocks from the Ordovician to the Carboniferous (Muñoz et al., 2002). The Miocene and Pliocene ignimbrites along with some Upper Paleozoic rocks outcrop on the slope of the Western Cordillera (Mpodozis et al., 2005).

The current depocenter of the basin is mainly filled by clastic and evaporite sediments that, due to the continuous lateral groundwater recharge coming from the mountains and permanent evaporation, have generated a nucleus enriched in sodium chloride of area 1360 km^2. The nucleus is surrounded by a marginal zone that corresponds to the intersection between the mixing zone and the land surface. The mixing zone has an area of approximately 2000 km^2, and it is constituted by halite, gypsum and calcite (Vásquez et al., 2013).

2.1. Hydrogeology

As an endorheic basin, all recharge that occurs in the aquifers of the Salar de Atacama is produced by infiltration of rainfall. Because the Andean Range acts as a barrier to the amazonian clouds and Humboldt Current of the Pacific coast, the Salar de Atacama is under a subtropical high-pressure zone, and it has a hyperarid climate that is characterized by low precipitation rates.

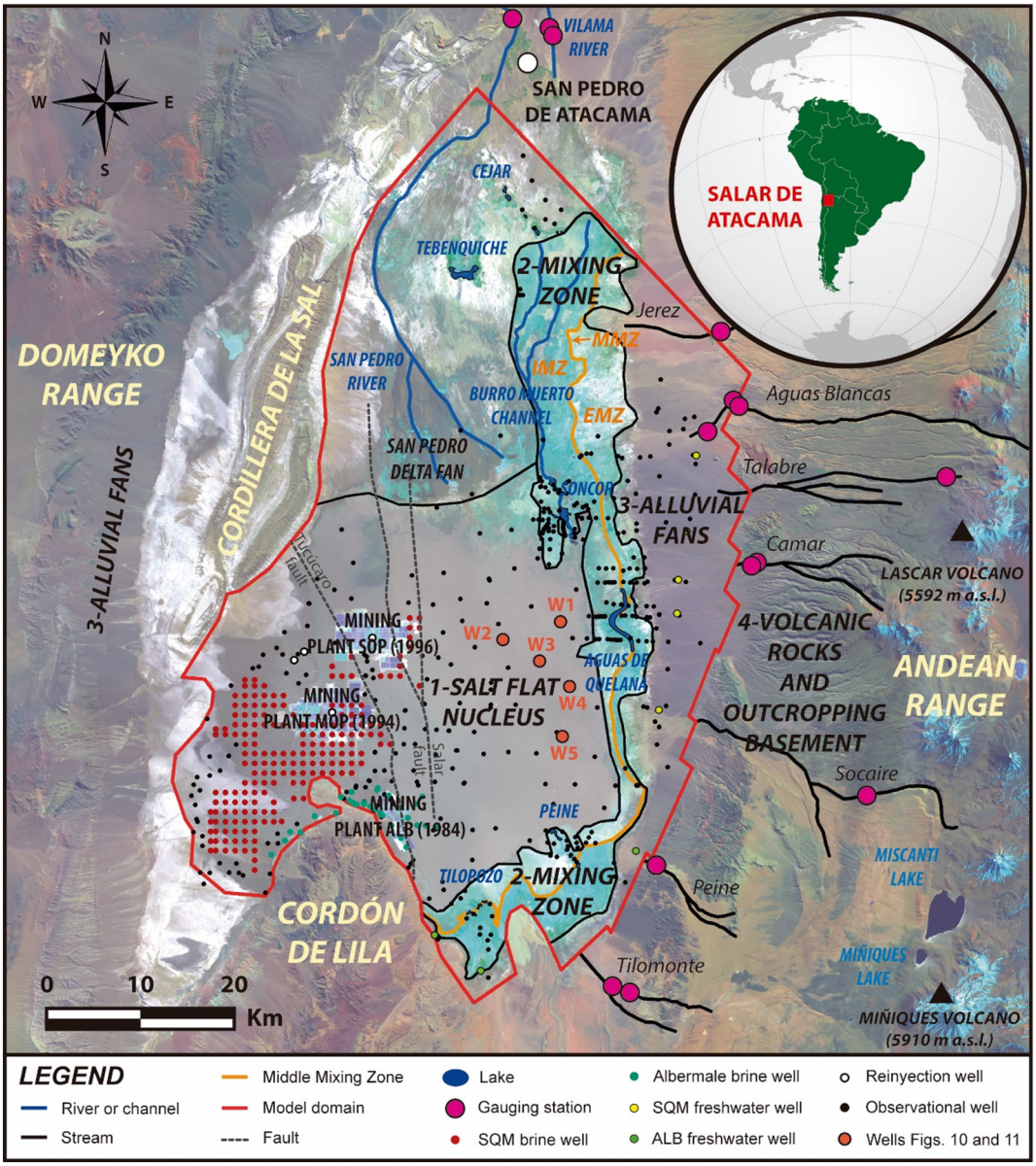

Fig. 1. Location of the Salar de Atacama (LANDSAT 8: 27 September 2016). The black lines border the salt flat nucleus and the mixing zone. The three sub-zones of the mixing zone are shown in orange lettering (internal, IMZ; middle, MMZ and external, EMZ). (For interpretation of the references to color in this figure legend, the reader is referred to the web version of this article.)

The surface water network is scarce, and the highest flows occur in the San Pedro and Vilama rivers (Fig. 1). The San Pedro River forms an alluvial fan (San Pedro alluvial fan) when arriving at the northern margin of the salt flat, where water infiltrates detrital sediments. Additionally, there are some intermittent streams that drain, across the eastern margin, the water from the mountains such as the Toconao, Aguas Blancas, Talabre, Camar, Socaire, Peine and Tilomonte streams. At a short distance from San Pedro alluvial fan, and in the east direction, the Burro Muerto Channel connects and feeds the Chaxa and Barros Negros Lakes which constitute the Soncor Lake system.

In addition to Soncor, there are several lakes (Cejar, Tebenquiche, Aguas de Quelana, Peine and Tilopozo) in the mixing zone associated with the upward flows that constitute highly valuable ecosystems that serve as a habitat or nesting centre for Andean flamingos and other species (Cornellà et al., 2009; Ortiz et al., 2014; Salas et al., 2010; Tejeda et al., 2003) (Fig. 2). Marazuela et al. (2018) differentiated three hydrodynamic zones inside the mixing zone: an internal mixing zone (IMZ), middle mixing zone (MMZ) and external mixing zone (EMZ). Most of the lakes are located in the upstream flows associated with the MMZ, which separates the IMZ from the EMZ (Fig. 1). The IMZ exhibits a hydrodynamics dominated by groundwater movements associated with density contrasts. On the other side, the EMZ is controlled by the groundwater flows coming from the recharge in the mountains (Marazuela et al., 2019). The water table depth in the natural regime ranges from 0.1–1 m in the salt flat nucleus and 0–1.5 m in the mixing zone.

In the nucleus, the most permeable aquifer is the upper stratigraphic unit of halite (Fig. 2) (IDAEA-CSIC, 2017; Marazuela et al., 2019). Below, a second halite aquifer is confined by a low permeability stratigraphic unit of gypsum that constitutes an intermediate aquitard. Towards the margins, the hydro-stratigraphic sequence aquifer-aquitard-aquifer is transferable to the alluvial fans as a regional simplification, where the upper and lower high-permeability detrital deposits are detached from the lower ones by a poorly permeable layer constituted mainly by sands, silts and ashes. Two main faults affect the thickness and geometry of these stratigraphic units, the Salar and Tucúcaro faults.

3. Materials and methods

In this section, the methodology followed to obtain the data used for the estimation and calibration of the inflows and outflows of the numerical model is described. First, the meteorological data considered for the estimation of recharge, evaporation and flow of streams are explained. Second, we address the hydrogeological data, which include the pumping rate of the brine and freshwater wells, the hydraulic heads of the observational wells and the hydraulic parameters involved in the calibration process of the numerical model. Finally, the geometry and performance of the 3D transient-state numerical model are described.

3.1. Meteorological data

3.1.1. Recharge

The rainfall data were provided by 14 weather stations located in the Salar de Atacama basin (see their locations in Fig. 3A). Some rainfall events affect a very local area, and analysing the rainfall over time in an integrated manner is not possible. Therefore, each rainfall event from January 1986 to December 2015 was mapped individually. Thus, an isohyets map of each event was created, taking into account topographic factors as the dominant criteria for the interpolation.

Two multivariate methods were used to fill gaps in the rainfall time series: weighted linear combination (Peterson and Easterling, 1994) and the Karl methodology (Karl and Williams, 1987). The first method allows filling the gaps from the data of statistically proximal series by means of a weighted linear combination of the series that are used. The second method replaces the gap of a record by the corresponding value of another nearby station that has a high linear correlation index, it being necessary to know the behaviour of precipitation in the basin (e.g. rainfall gradient).

The recharge by infiltration of rainfall water was calculated by subtracting the detention from the total precipitation following the criteria of Marazuela et al. (2019). In accordance with this previous work, the Salar de Atacama basin cannot be treated as a typical hyperarid area with very low infiltration rates and a homogeneous precipitation rate. The sparse vegetation, the underdeveloped surface water network and the high degree of fracturing of the rocks of the mountains (the main recharge area) imply that the great part of the rainfall infiltrates in the mountains. Detention is the proportion of rainfall that will not arrive to infiltrate and recharge the aquifers. At the beginning of each precipitation event, approximately 5 mm are detained in the soil and return to the atmosphere by evaporation. This value is justified because rainfall events lower than 5 mm almost never affect the water table of the salt flat because the water is detained in the soil and subsequently evaporated. This value was subtracted for each rainfall event.

The zoning to quantify the recharge by rainfall was performed at two levels: (1) peripheral sub-basins and (2) the salt flat nucleus, mixing zone and alluvial fans. The first correspond to the most elevated areas

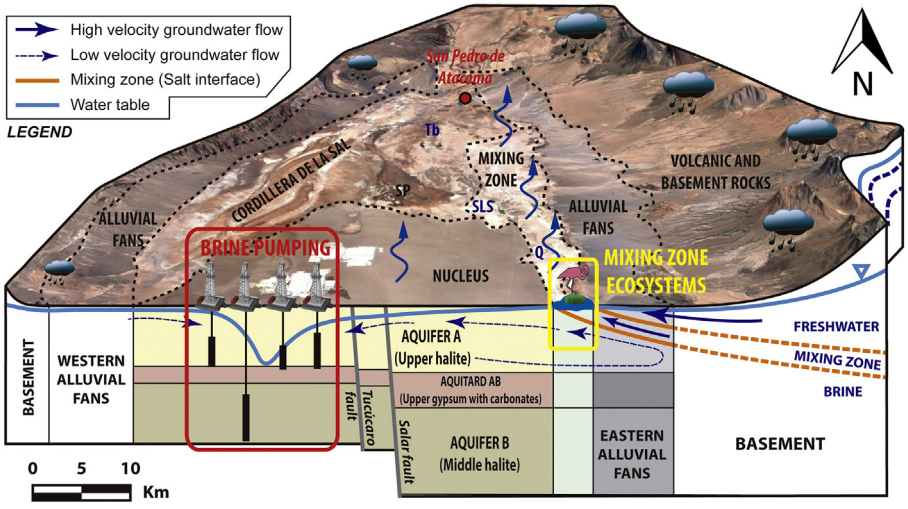

Fig. 2. Hydrogeological performance of the Salar de Atacama basin (modified from Marazuela et al., 2019). Q is the Quelana Lake, SLS is the Soncor Lake system, Tb is the Tebenquiche Lake and SP is the San Pedro alluvial fan.

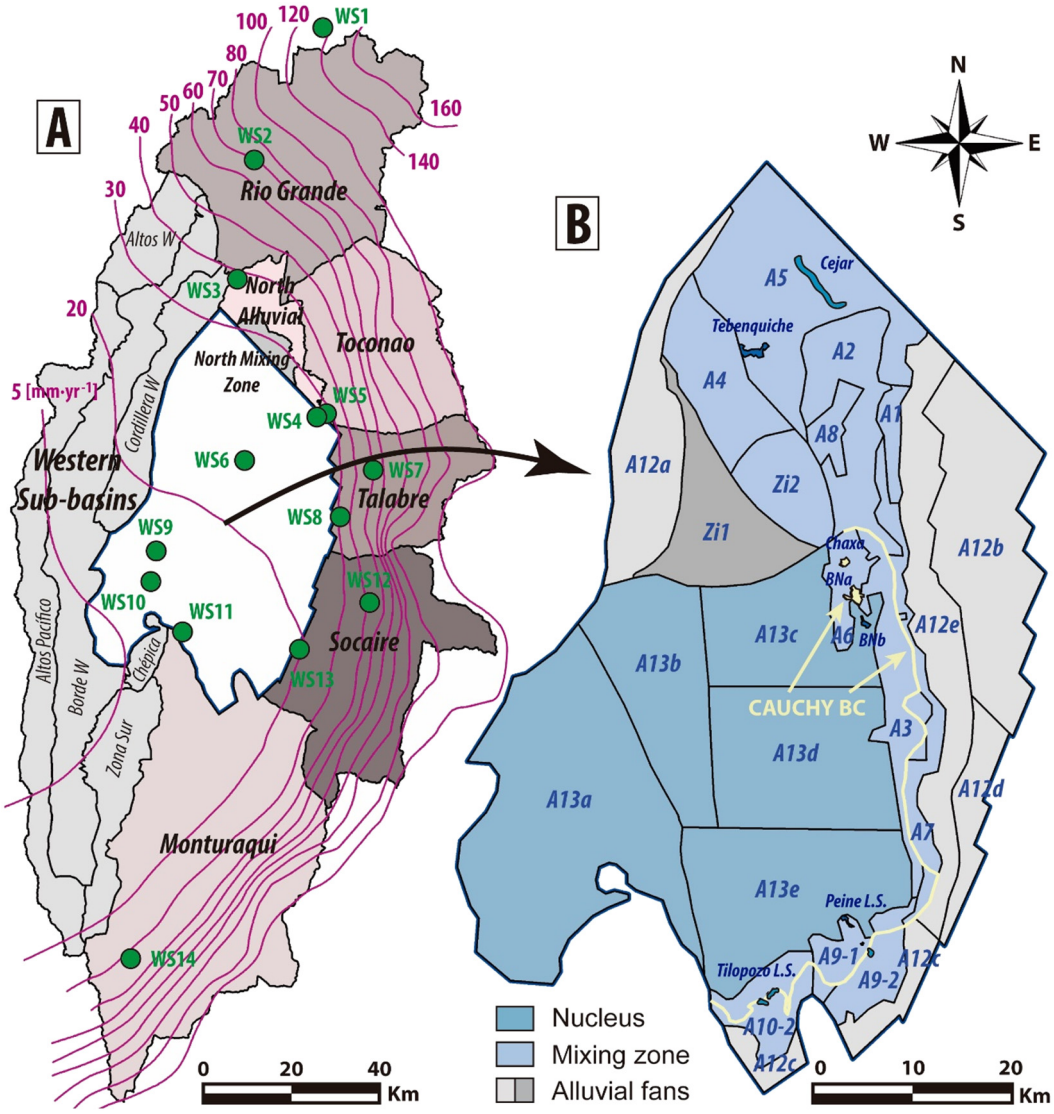

Fig. 3. Superficial recharge and evaporation zones (modified from Marazuela et al., 2019). A) Regional recharge sub-basins and isohyets map. Green points indicate the positions of the weather stations. The basin recharge values of each zone are listed in Table S1. B) Recharge zones at the surface of the model domain. The recharge and evaporation values of each zone are listed in Table S2. (For interpretation of the references to colour in this figure legend, the reader is referred to the web version of this article.)

located between 2400 and 5500 m a.s.l. The sub-basins of greater extension and elevation are found in the eastern half of the basin. In these areas, andesite and ignimbrite rocks appear interspersed with continental sedimentary facies. They constitute aquifers of low hydraulic conductivity and storage capacity, although they can increase their effective hydraulic conductivity due to the high degree of fracturing. As explained above, the high degree of fracturing together with the scarce vegetation and the processes of physical-chemical weathering on the surface make the infiltration rate very high. A total of 11 sub-basins were defined based on a morphometric study that included a digital elevation model and satellite images (LANDSAT 7 and 8) (Fig. 3A). On the other hand, the domain that encompasses the salt flat nucleus, mixing zone and alluvial fans was discretized into 30 zones according to geomorphological and soil features (Fig. 3B). The recharge values for sub-basins are listed in Table S1, and those for surface zones are presented in Table S2.

3.1.2. Evaporation

The evaporation in the Salar de Atacama occurs from the water table which is very close to the ground (phreatic evaporation). The higher evaporation rates, however, occur in the mixing zone where the water table is closer to the land surface and where some lakes allow direct evaporation. In the salt flat nucleus, the polygonal structure of the salt crusts allows the rise of the groundwater by capillarity and favours evaporation from the water table when it is close to the surface. Although the evaporation rate in the nucleus is much less than in the mixing zone, this should not be neglected because the surface area is very large.

Evaporation rates were estimated from the experimental data registered by evaporation trays and lysimeters. Evaporation trays were installed in the weather stations. Lysimeters were installed in the mixing zone to measure the evaporation from the groundwater. Evaporation rates were correlated with the water table depth by fitting the experimental data of the lysimeters with the Philip (1957)-type curve. This method relates the evaporation rate that is measured to the water table depth through an exponential fit.

Considering the characteristics of each type of soil and the data collected by the evaporation trays, the annual evolution of the evaporation rate in each zone of the Fig. 3B was established. The average values for each zone are listed in Table S2.

3.1.3. Streams

Although the surface water network is undeveloped in the Salar de Atacama basin, two rivers and some streams may be identified. Streams descend from the eastern mountains until the alluvial fans, where the often intermittent flows infiltrate as a consequence of the high permeability. These streams were continuously monitored using 15 gauging stations (see their locations in Fig. 1). Time series gaps were filled through data correlation between nearby gauging stations, taking into account the average value of each stream and the meteorological data of the weather stations. The highest flows are in the San Pedro River, with 0.72 $m^3 \cdot s^{-1}$, and the Vilama River, with 0.28 $m^3 \cdot s^{-1}$, both of them at the north of the Salar de Atacama. The other streams, such as Toconao, Aguas Blancas, Talabre, Camar, Socaire, Peine and Tilomonte, are located on the eastern or south-eastern side of the Salar de Atacama, with flow rates that range between 0.15 $m^3 \cdot s^{-1}$ and 0.01 $m^3 \cdot s^{-1}$. The average values of streams are presented in Table S3.

3.2. Hydrogeological data

3.2.1. Pumping wells

At present, two mining companies pump the brine of the Salar de Atacama. These companies are Sociedad Química y Minera de Chile S.A. (SQM), owner of mining plants MOP and SOP and Albemarle Corporation (ALB), owner of mining plant ALB.

The pumping network of SQM consists of several hundred brine pumping wells located in the southwestern salt flat nucleus, 5 freshwater wells in the eastern alluvial fans and 4 reinjection points associated with infiltration from the evaporation pools (Fig. 1). Daily flow rates are available from the beginning of the pumping in 1994.

The pumping network of the ALB mining company comprised 62 brine wells in the southern salt flat nucleus and 3 freshwater wells in the southern alluvial fans. Historical flows were seasonally represented based on the data presented in Rockwood-Lithium (2015).

The brine pumping performed by ALB began in 1983 at a rate of 0.05 $m^3 \cdot s^{-1}$ and increased to 0.13 $m^3 \cdot s^{-1}$ by 2015. The extraction of brine performed by SQM began in November 1994 at a rate of 0.07 $m^3 \cdot s^{-1}$ and reached 1.37 $m^3 \cdot s^{-1}$ in 2015, with the maximum extraction in summer and minimum in winter (Comisión Regional del Medio Ambiente, 2006; IDAEA-CSIC, 2017). The freshwater pumping performed by ALB ranged between 0.01 $m^3 \cdot s^{-1}$ in 1999 and 0.02 $m^3 \cdot s^{-1}$ in 2015, and for SQM, it ranged between 0.07 $m^3 \cdot s^{-1}$ in 2000 and 0.21 $m^3 \cdot s^{-1}$ in 2015. The SQM reinjections increased from 0.1 $m^3 \cdot s^{-1}$ in 1996 to 0.38 $m^3 \cdot s^{-1}$ in 2015. Therefore, a pre-operational period (1986–1994) and an operational period (1994–2015) were differentiated. In the pre-operational period some brine extractions occurred, but they were insignificant compared with those that have occurred since 1994.

3.2.2. Observational wells

The hydraulic head time series were recorded manually or with a data logger in a total of 549 wells (see their locations in Fig. 1). The data were corrected for variable density variations following the methodology of Marazuela et al. (2018). This methodology is based on the application of a correction to the fresh and mixed water heads to compensate for the density variations, taking as reference the density of the brine (1.23 $kg \cdot L^{-1}$).

3.2.3. Hydraulic parameters

Evaporites and cemented detrital deposits of salt flats have low hydraulic conductivities if they are not altered. However, the dissolution and karstification increase the permeability by several orders of magnitude, resulting in preferential channels (Bakalowicz, 2005). These deposits can be treated as discretized equivalent porous media in regional studies (Scanlon et al., 2003).

The reference values of the hydraulic conductivity and specific storage were deduced from the hydraulic tests performed by mining companies and in some cases reinterpreted by other authors (IDAEA-CSIC, 2017; Marazuela et al., 2019; Rockwood-Lithium, 2015). The zoning of the hydraulic parameters and specific storage was performed based on lithological and soil features, pumping test results and the previous study (Fig. 4).

3.3. Numerical modelling

A transient-state groundwater flow model was constructed to reproduce the hydrogeological behaviour of the Salar de Atacama between January 1986 and December 2015, considering the natural (recharge and evaporation) and anthropogenic processes (freshwater and brine pumping and reinjections). For the initial condition, the steady-state water table presented by Marazuela et al. (2019) was used, which represents the average hydraulic heads in the natural regime, prior to brine pumping, similar to the 1986 regime. A time step limited to 10 days was applied. The FEFLOW code (Diersch, 2014) was used to solve the three-dimensional groundwater flow equation.

3.3.1. Model set-up

The model domain (Fig. 1) has an area of 3303 km^2 and covers the salt flat nucleus, the mixing zone and a large part of the eastern alluvial fans. The eastern boundary is the contact between the alluvial fans and the basement or volcanic rocks, the southern boundary is the contact between the salt flat nucleus and the Cordón de Lila, the western boundary is the contact with the Cordillera de la Sal which is constituted by oligocene-miocene evaporites, and the northern boundary correspond with a deep structural lineament, sufficiently far from the area of interest (IDAEA-CSIC, 2017).

The three-dimensional mesh contains four layers with a total of 266,340 triangular prism elements to represent aquifer A, aquitard AB and aquifer B (Fig. 5). Aquifer A and aquitard AB are represented with one layer each. Aquifer B is represented through the two lower layers to correctly reproduce the strong fault jump caused by the Salar fault. The mesh is refined near fault jumps, lakes, pumping wells and observational wells. The sizes of the elements range between 10 and 300 m.

3.3.2. Boundary conditions

The lateral groundwater recharge that represents the flows coming from the water recharged in the mountains was implemented through the well-type boundary condition around the domain for each subbasin. Due to the distance between the mountains and the model domain and due to the thick unsaturated zone in the mountains, these values were constant over time. The recharge produced by the rainfall events that occurred directly in the model domain, due to the thin unsaturated zone, was incorporated as a Neumann-type boundary condition. Therefore, for each defined recharge zone on the top boundary of the model, a time series with the estimated recharge values of each rainfall event was obtained.

The evaporation was incorporated through double boundary conditions, outflow on top and Cauchy-type. The outflow on top was used to implement the time series of the evaporation rate in each zone of the nucleus and mixing zone, including lakes. The evaporation time series included a progressive non-linear reduction in the salt flat nucleus due to the deepening of the water table produced by the pumping. The Cauchy-type boundary condition with a high leakage served to prescribe the hydraulic head in the Soncor Lake system and in the MMZ, where the water head was similar to the salt flat nucleus over time. The northern stretch of the mixing zone mapped in Fig. 1 was not taken into account for the Cauchy boundary condition (Fig. 3B) because the water heads change with respect to the nucleus, and it would be necessary to apply density corrections to the prescribed water heads. The outflow from this zone was considered based on the calibrated value of the Neumann-type boundary condition.

Finally, a well-type boundary condition was used to reproduce the extractions and reinjections. The brine pumping wells were adjusted

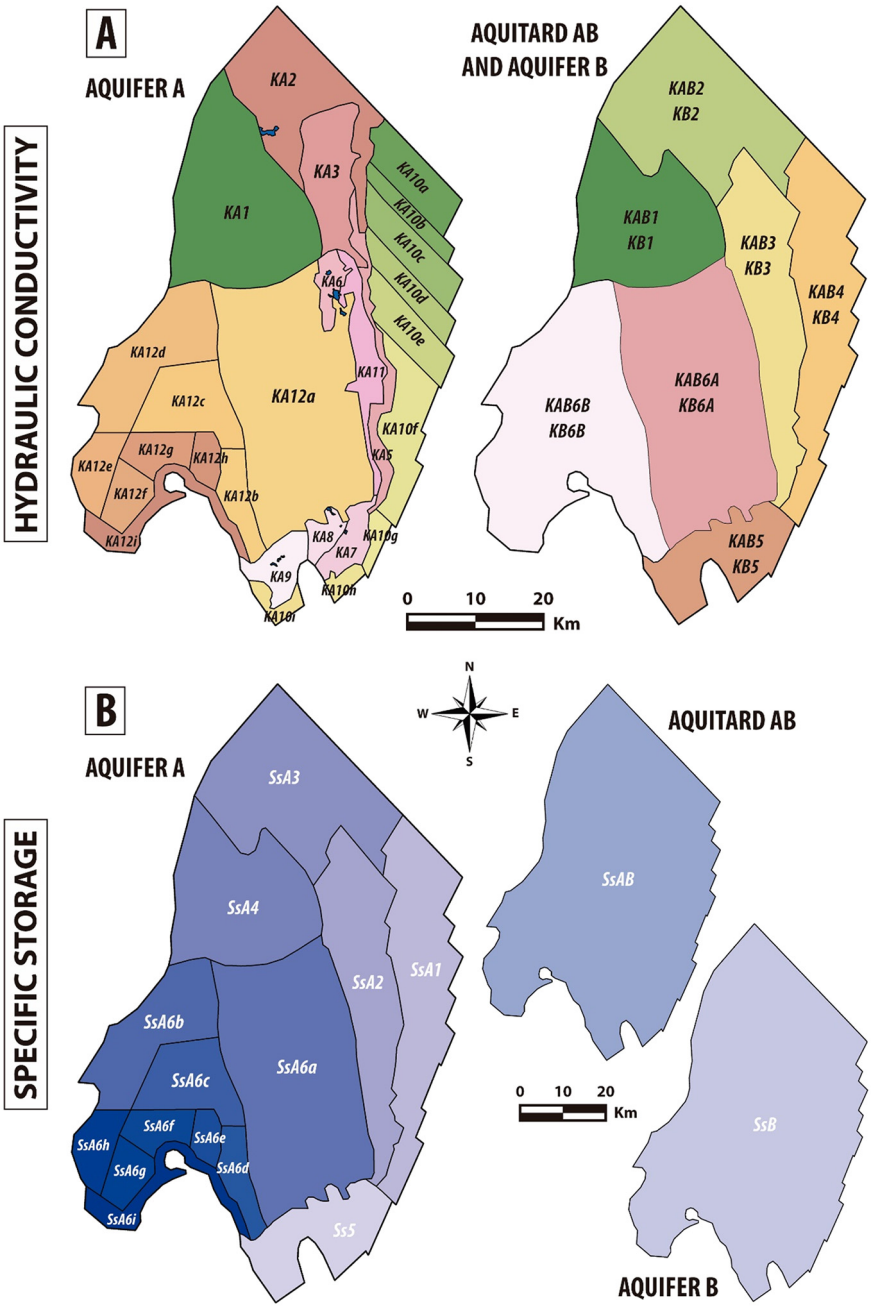

Fig. 4. Zoning of the hydraulic conductivity (A) and specific storage (B) for each hydrogeological unit (modified from Marazuela et al., 2019). The hydraulic conductivity values are listed in Table S4 and the specific storage values in Table S5.

to a simplified network of equivalent wells to facilitate their implementation in the numerical model. This network of equivalent wells was made using a regular mesh with cells of 1 km^2 resolution, assigning the accumulated pumping of the wells in each cell to its centroid (Fig. 6). This methodology was performed independently for aquifer A and aquifer B. A total of 245 equivalent wells were used.

3.3.3. Model calibration

The calibration process was performed through inverse modelling with the parameter estimation code PEST (Doherty, 2015). The core of the PEST engine is the Gauss-Levenberg-Marquardt algorithm (GLMA), which iteratively optimizes the model parameters to improve their fit to observed data by means of an objective function.

The calibration of the hydraulic conductivity, lateral recharge and average evaporation was a joint process based on the steady-state model of Marazuela et al. (2019). The specific storage was calibrated for the transient-state model.

The hydraulic conductivities in aquifer A exhibited values ranging between 80 and 300 $m \cdot d^{-1}$ for the alluvial fans and between 60 and 300 $m \cdot d^{-1}$ for the salt flat nucleus and mixing zone (Table S4). The hydraulic conductivities in aquitard AB ranged between 0.01 and 5 $m \cdot d^{-1}$, and in aquifer B, they ranged between 0.1 and 20 $m \cdot d^{-1}$. The specific storage values (Table S5) ranged between 0.007 m^{-1} and 0.012 m^{-1} in aquifer A. For aquitard AB and aquifer B, the specific storage was 10^{-4} m^{-1} and 10^{-5} m^{-1}, respectively.

4. Results and discussion

In this section, the field data combined with the results of the 3D transient-state numerical model are used to discuss the natural

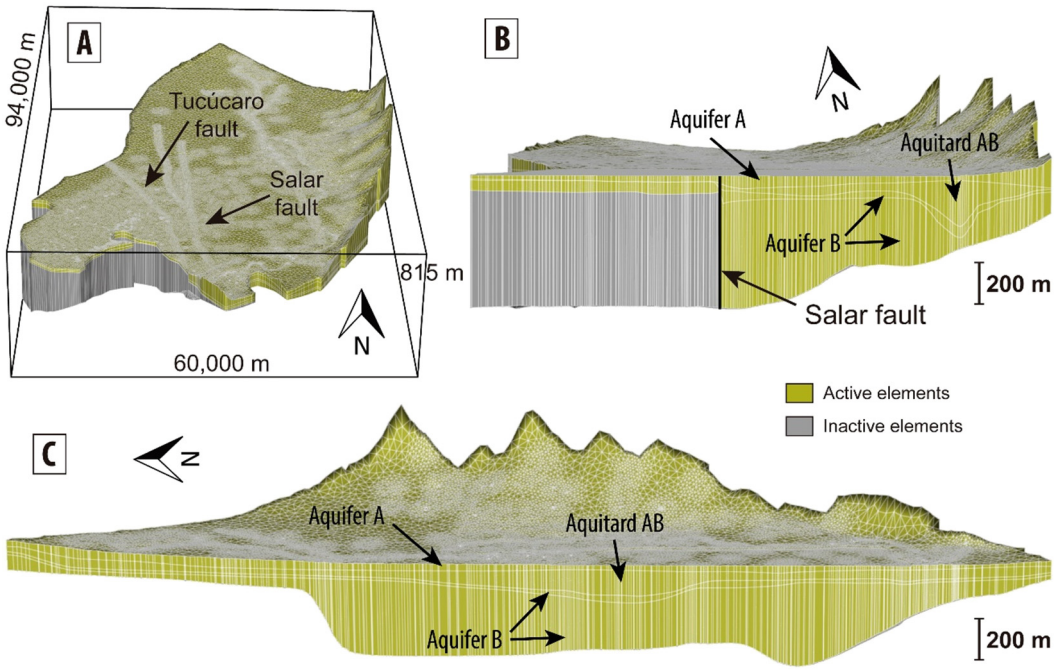

Fig. 5. Mesh of the 3D numerical model. A) 3D view. B) East-West vertical cross section. C) North-South vertical cross section.

hydrodynamics of the Salar de Atacama and how the brine pumping has impacted the natural water table to abstract patterns applicable to other salt flats.

First, the individualized natural processes, recharge and evaporation, that occurred in the Salar de Atacama and their coupled behaviour are addressed separately. Subsequently, the effects that caused brine pumping are evaluated and discussed to extrapolate general patterns to other salt flats.

4.1. Natural hydrodynamics of the Salar de Atacama

The results of the numerical model simulation show the evolution of the water table of the Salar de Atacama from 1986 to 2015, taking into account the brine pumping (Figs. 7 and 8). The brine pumping was almost non-existent until 1994, and therefore it is very interesting to first establish the natural hydrodynamics of the salt flat during this period (1986–1994) to be able to discuss in the following section the anthropogenic impacts of brine pumping.

In the natural regime, the water table is controlled by evaporation and recharge processes. The experimental data reveal that the evaporation has a clearly seasonal behaviour, with average minimum values of 1050 $mm \cdot yr^{-1}$ from June–July and maximum values of 4450 $mm \cdot yr^{-1}$ from December–January. In addition to this annual evaporation wave, there is a daily day-night cycle that also modulates the evaporation rate. These values decrease exponentially until extinguishing at water table depths between 0.5 and 2 m, as evidenced by the lysimeter data (Fig. 9).

The evaporation process is apparent in the water table evolution mainly as an annual cycle. Thus, the greater evaporation in summer than in winter causes a gradual drawdown from December to June and a gradual rise from June to December. The phase of the sinusoidal effect may change slightly depending on the salt flat zone if any external factor, such as the lateral groundwater recharge that arrives from the mountains, generates a change in the water table depth. In Fig. 10, the correlation between the hydraulic heads and the normalized evaporation function applied for each average value of evaporation is shown. This normalized function was computed based on the evaporation data of the open water reservoir (evaporation trays data). The water table oscillations due to the annual cycle of evaporation reach a half metre in the mixing zone, where the water table is closest to the topographic surface and the evaporation rate is higher (Fig. 8). However, in most modelled areas the maximum oscillation caused by evaporation is centimetres or a few decimetres. This effect can be observed in detail in the observed and modelled hydraulic heads shown in Fig. 8 during the pre-operational period. The wells P1, P2 and P3 located in the north-eastern mixing zone exhibit higher oscillation ranges due to evaporation, which is approximately 0.10 to 0.50 m. Additionally, the annual cycle of evaporation is evidenced in the wells P5, P10 and P11, with amplitudes from approximately 0.10 to 0.30 m for the eastern and south-eastern mixing zones. Furthermore, during the pre-operational period, this cycle is also evidenced in the wells P4, P6, P7 and P9 of the brine pumping area, with oscillation rates between 0.10 and 0.20 m. These field data confirm that in the natural regime, both

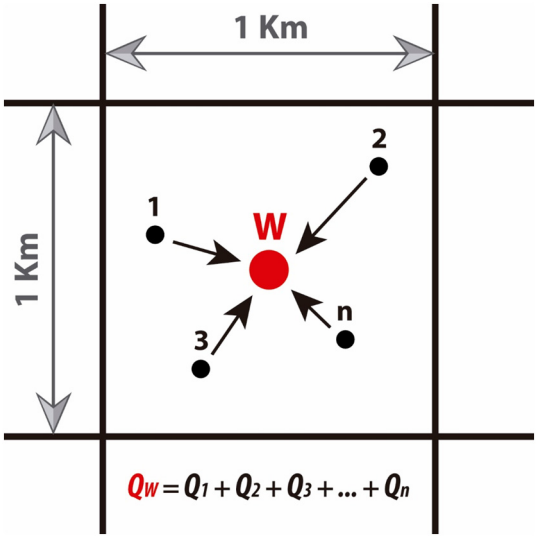

Fig. 6. Methodology used for the definition of the equivalent wells.

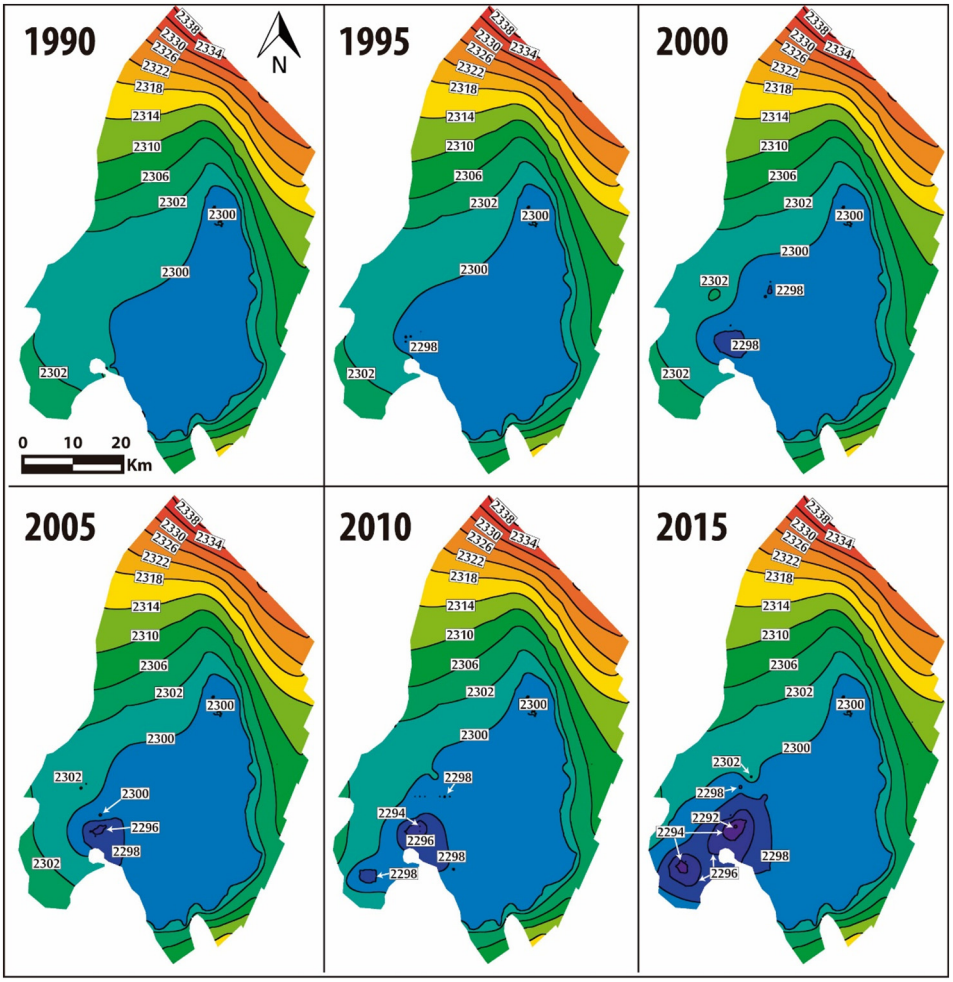

Fig. 7. Hydraulic head contour maps resulting from the 3D transient-state numerical model. The results are shown every five-year periods from December 31st, 1990 to December 31st, 2015. The black letters indicate the value of each hydraulic head contour line in meters above sea level (m a.s.l.).

the nucleus and the mixing zone evaporated the groundwater. The mixing zone experienced a higher evaporation rate due to the shallower water table and the existence of lakes connected to the water table. This is coherent with the lower amplitude of the evaporation cycle in the salt flat nucleus relative to the mixing zone.

The meteorological data provided by the weather stations reveal that rainfall rate ranged from <10 mm·yr^{-1} in the salt flat nucleus to >160 mm·yr^{-1} in the eastern mountains (Fig. 3A). The rainfall events are very scarce, and they are concentrated from December to March. The amount of precipitation is controlled by the climatic cycles, and it is subject to cycles of 5, 10 or more years, coinciding also with the El Niño – Southern Oscillation (ENSO). In the salt flat nucleus, the precipitation decreases from north to south and from east to west, since the clouds discharge the water before reaching the south-western end of the salt flat.

The effect of the rainfall recharge on the water table depends on its location. Rainfall events can occur both directly on the salt flat nucleus and mixing zone or in the mountains. An abrupt and instantaneous rise in water table is observed with each direct rainfall event on the salt flat nucleus and the IMZ due to the small thickness of the unsaturated zone. However, some rainfall events exhibit no direct impact on the water table or a linear relationship between the amount of rainfall and the disturbance of the water table (Fig. 11). This behaviour is a consequence of the type of soil, the spatial distribution of the rainfall event and the temporal lag between rainfall events which modify the detention. Owing to the great extent of the basin, the rainfall events did not present a homogeneous distribution along the entire basin, making it necessary to analyse the isohyets map for each event and translate this into the time series of the numerical model. Thus, rainfall events with high rainfall rates and great spatial extent (rainfall events identified at several weather stations) are those that give rise to greatest abrupt rises of the water table (Fig. 11). This type of perturbation can trigger abrupt ascents of several decimetres of the water table, as observed in Figs. 8 and 11. Black arrows denotes each of the rainfall events than caused a strong rise of the water table, with eight being the most important during the last 30 years.

Regarding the rainfall events that occurred in the mountains, however, the perturbation that they produced in the water table of the salt flat is not obvious. There, the rain water infiltrates the soil and recharges aquifers. The amount of water recharged in the eastern mountains is very large due to the low detention in the soil caused by the presence of fractured soils (ignimbrites) and the scarce vegetation. However, despite the large volume of water recharged, the perturbations to the water table were not evident in the salt flat. This is because due to the greater thickness of the unsaturated zone in the mountains and the distance from the mountains to the salt flat nucleus, the effect of the rainfall events is damped.

In the salt flat nucleus and the IMZ, the coupling of both natural processes, evaporation and recharge, results in a water table evolution dominated by a gradual decay due to evaporation which is disrupted by sudden level rises caused by episodic rainfall events. The natural trend of the water table is to gradually decay because the evaporation

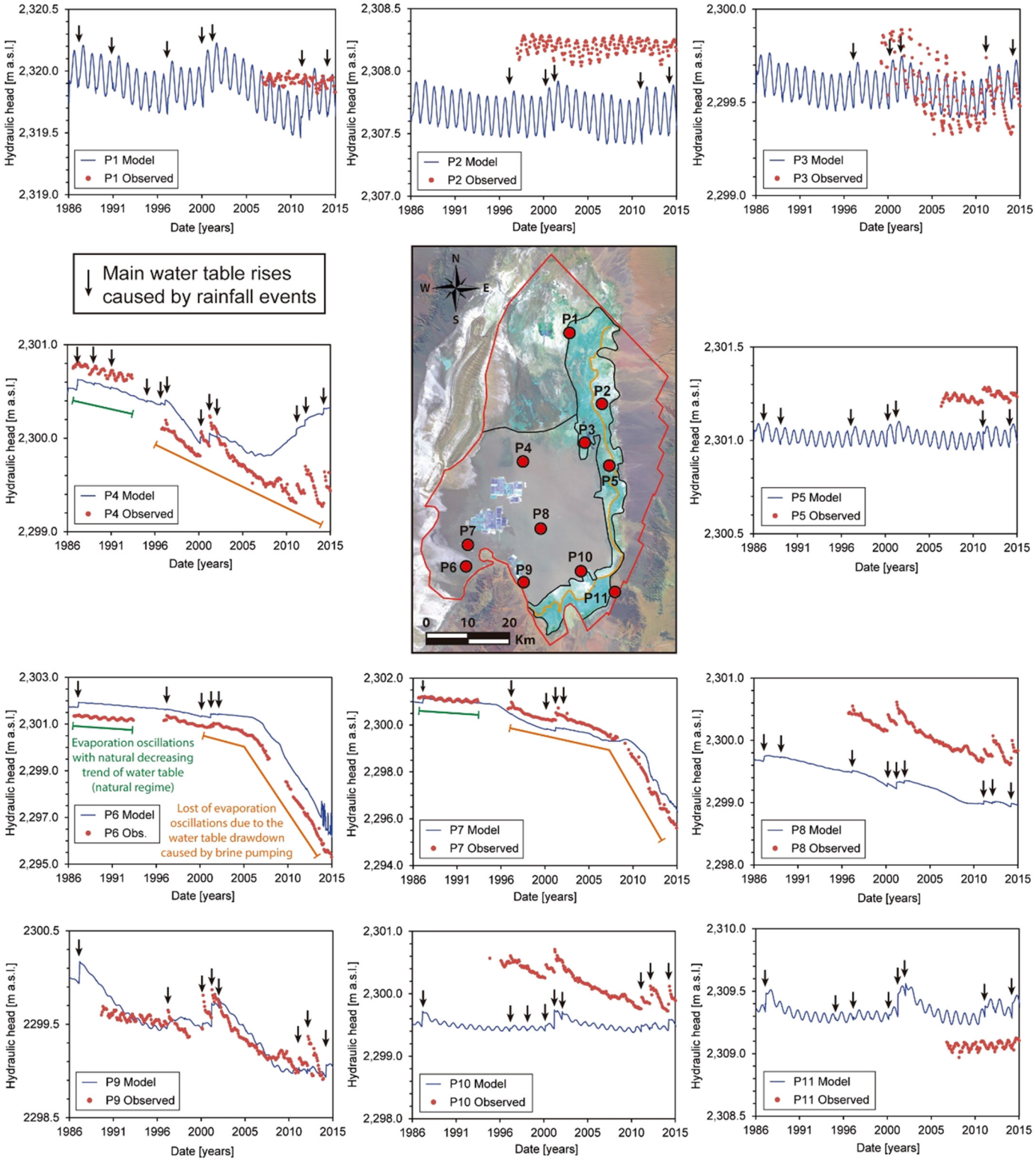

Fig. 8. Hydraulic head evolution at eleven observational wells showing the modelled versus measured (observed) data. The measured data outside the mixing zone were corrected for density variations following the methodology of Marazuela et al. (2018). The location of the piezometers are shown in the centre of the figure.

is greater than the recharge for most of the time period studied. This effect is evidenced by the evolution of the hydraulic heads of the P4, P8, P9 and P10 wells (Fig. 8), where the decreasing natural trend due to evaporation is only perturbed by the episodic rainfall events.

In the EMZ, the gradual decay caused by evaporation is damped even though the evaporation rate is the highest. This is because the mixing zone acts as a hydraulic barrier that isolates the two systems, the salt flat nucleus and the IMZ on one side and the main recharge area (mountains), the alluvial fans and the EMZ on the other, with the domains separated by the MMZ. In the EMZ, the rainfall events did not exhibit such a direct response in the water table, especially those far away from the intersection of the mixing zone with the land surface. The lateral

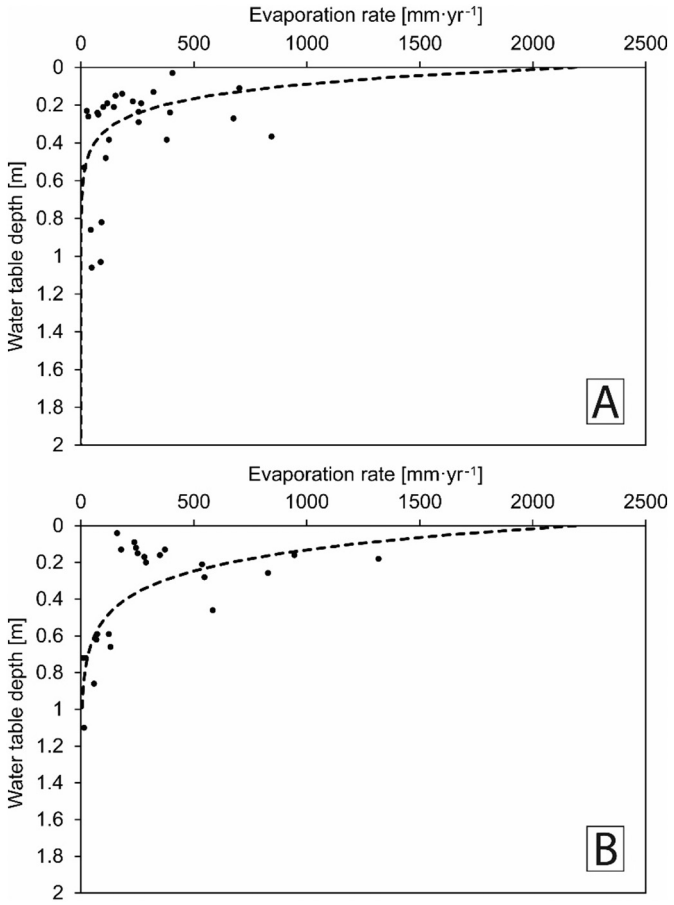

Fig. 9. Experimental data of evaporation rates taken by lysimeters located in the evaporation zones A3 and A7. The fit of the average exponential curve was based on the Philip (1957) type curve.

groundwater recharge dominates the surface recharge, and the unsaturated zone becomes wider, weakening the direct effect of the rainfall. This process results in fairly constant hydraulic heads over time even though they are affected by evaporation and surface recharge (see the evolution of the hydraulic heads of the P2, P3 and P5 wells in Fig. 8).

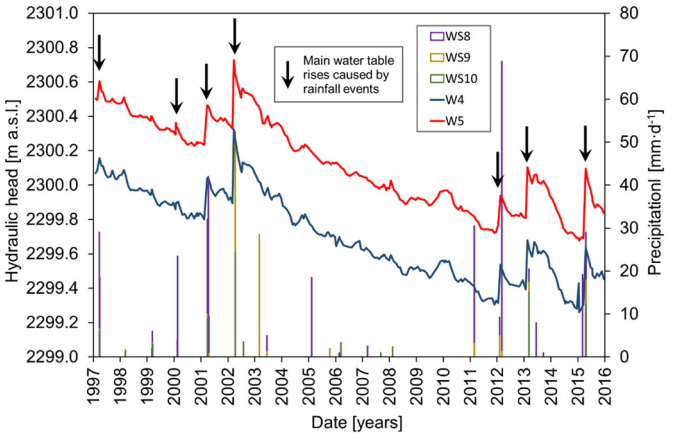

Fig. 11. Correlation between rainfall events registered at three weather stations (WS8, WS9 and WS10) (see their locations in Fig. 3A) and the hydraulic head values of the observational wells W4 and W5 (see their locations in Fig. 1).

As a consequence of the barrier effect exerted by the mixing zone, the hydrodynamics of the salt flat nucleus and the IMZ are those of pools that are quasi-isolated from the groundwater that arrives from the mountains as lateral recharge. The groundwater movement in these areas (nucleus and IMZ) is much slower and is controlled mainly by density-driven forces.

4.2. Anthropogenic impacts

Under the natural regime, evaporation and recharge control the hydrodynamics and water table of the salt flat. However, in the Salar de Atacama there has been intensive brine exploitation, whose potential impacts on the natural hydrodynamics require analysis and quantification to extrapolate its behaviour to other salt flats.

4.2.1. Water table evolution

The water table evolution results from the numerical model shows the origin and evolution of different water table drawdowns as a consequence of the pumping of brine (Figs. 7 and 8). Prior to 1994, the brine pumping performed in the southern area of the salt flat nucleus by ALB did not produce large disturbances in the natural regime. In 1994, the first effects of the pumping appeared, although they were still incipient

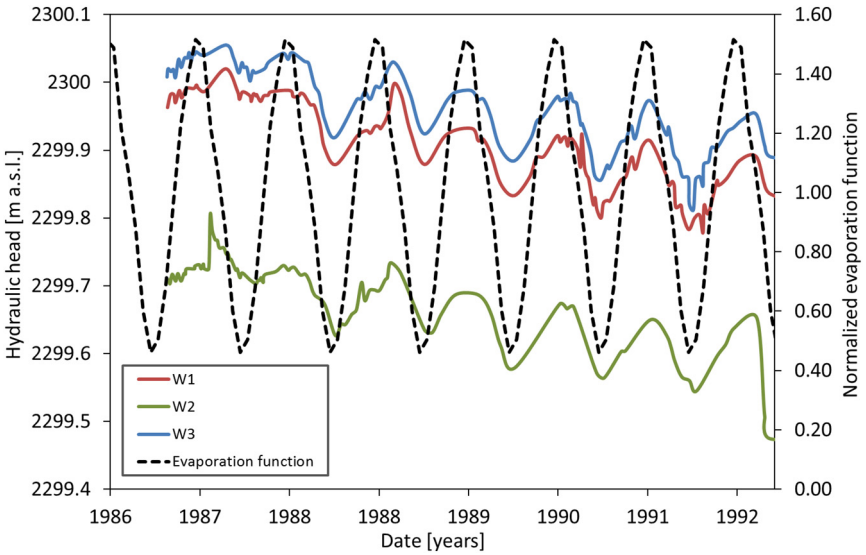

Fig. 10. Correlation between hydraulic head data from observational wells W1, W2 and W3 (see their locations in Fig. 1) and the normalized evapotranspiration function.

and only located in the southern zone of the nucleus. In 2000, the affected area spread and more acute pumping depressions developed in the southern area. In addition, the effects of the reinjections in the central-western zone of the nucleus were also evident. This situation was accentuated in 2005, when the southern water table drawdowns caused water heads lower than 2296 m a.s.l. In 2010, the southern drawdown cone continued to increase, and a new cone of depression was evident in the south-western sector. Both cones reached minimum hydraulic heads in 2015, with values below 2292 m a.s.l.

This gradual drawdown of the water table produced a change in the location of the regional minimum hydraulic head, which moved from the eastern mixing zone or close to it to the southwestern salt flat nucleus (the main brine pumping area). However, the water heads in the mixing zone and outdoor areas remained practically constant throughout this period. This is the same as saying that until now, the salt flat nucleus has been the only one that has clearly suffered the effects of brine pumping. This may be explained by both the isolating effect of the mixing zone already described above and the important reduction of the evaporation rate in the nucleus caused by the drawdown of the water table. Indeed, as the evaporation rate from the groundwater is a function of the water table depth, the brine pumping causes an exponential decay in the evaporation rate, which results in a dampening of the water table. This effect of the water table is clearly evidenced in the piezometers P7 and P8 (Fig. 8), which are located in the pumping area. The hydraulic heads of these piezometers clearly described the annual oscillations of evaporation during the pre-operation period, similar to the piezometers located far from the influence area of the pumping, but during the operational period, these oscillations disappeared as a consequence of the drawdown of the water table, indicating that evaporation process stopped as a result of the brine pumping. It is undeniable that the dependence of the evaporation rate on the water table depth enables any salt flat to counterbalance the increase and decrease of the entries of their basins. This makes salt flats and their ecosystems fairly stable over time on a geological scale, since wet periods with more rainfall would imply a rise in the water table that would automatically trigger an increase in the evaporation rate and therefore slow down this water table rise. In the same manner, a drier period would lead to inflows reduction in the basin due to rainfall, which would lead to a drawdown of the water table. The decrease in water table would cause a reduction in evaporation rate, which would slow down this water table drawdown. This effect is termed in the present work the *damping capacity* of the water table, which is a property of all salt flats that acts attenuating both natural and anthropogenic oscillations.

The damping capacity of the salt flats water table for natural oscillations is partially effective for anthropogenic perturbations of the basin water balance. However, to understand how the damping capacity responds to anthropogenic disturbances generated by brine pumping, it is necessary to delve into how the water balance has evolved at the basin scale during its transition. Thus, brine pumping beyond the natural evaporation outflow would cause irreversible depletions of the water heads until recharge was able to replace the pumped brine.

4.2.2. Water balance evolution

Therefore, it is necessary to analyse the water balance evolution computed by the 3D numerical model during the pre-operational and operational periods to advance the knowledge of the damping capacity of a salt flat when anthropogenic perturbations occur. First, the evolution of each inflow and outflow of the basin during the natural and the mining regimes is shown and discussed. Second, the effects of brine pumping in the water balance and the counterbalance that the damping capacity has produced in water balance are evaluated.

In the case of Salar de Atacama, the system was dominated by a negative water balance, which was counteracted punctually with rainfall events, especially during wet periods. The total inputs along the modelled period were $1.39 \cdot 10^{10}$ m^3, and the total outputs

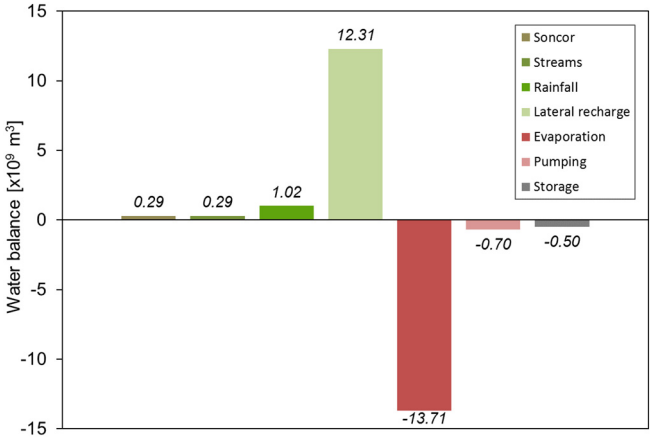

Fig. 12. Total water balance resulting from the 3D transient-state numerical model.

were $1.44 \cdot 10^{10}$ m^3 (Fig. 12). The resulting negative imbalance was $5.00 \cdot 10^{8}$ m^3, which was less than the volume of pumped brine.

As observed in the total water balance of the numerical model for the period from 1986 to 2015 (Fig. 12), 89% of the inflows to the salt flat were produced through the deep lateral recharge from the water infiltrated into the mountains. The remaining 11% comprised rainwater fallen directly on the domain (7%), infiltration from streams (2%) and infiltration from the overflow of the Soncor Lake system (2%).

The outflows of the system were produced by evaporation (95%) and by extraction of brine (5%). The Cauchy-type boundary condition exhibited adequate performance as the inflow produced through this boundary condition was <5% of the outputs, and both remained constant during the total modelled period.

The temporal evolution of the inflows, outflows and storage over time is shown in Fig. 13. The annual inflows oscillated between 13.54 m$^3 \cdot$s^{-1} and 17.31 m$^3 \cdot$s^{-1}, whereas the outflows had a lower oscillation range, between 14.46 m$^3 \cdot$s^{-1} and 15.82 m$^3 \cdot$s^{-1}. The inflows to the system were mainly represented by the rainwater recharge, which

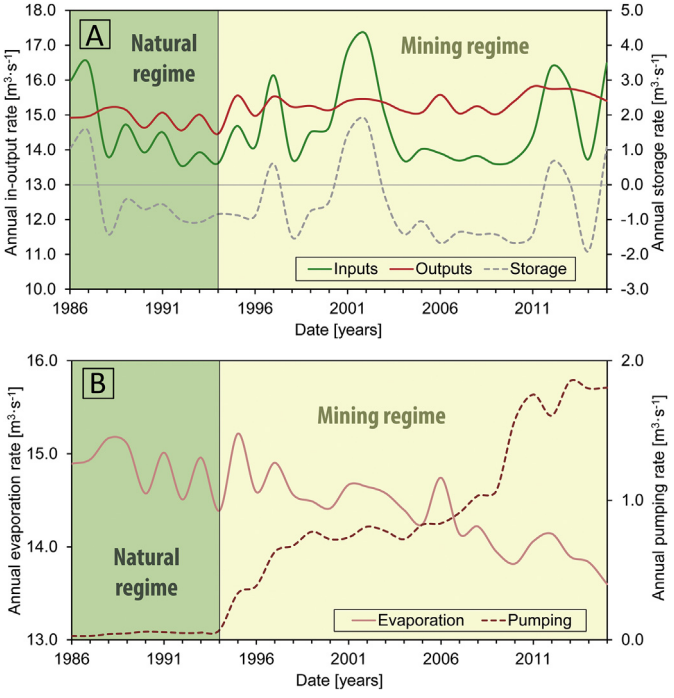

Fig. 13. Water balance evolution. Continuous lines correspond to the primary vertical axis and dashed lines correspond to the secondary vertical axis. A) Total inputs, outputs and storage rates. B) Total evaporation and pumping rates.

depends on the climate cycles. This results in inflow oscillations over time. On the other hand, the evaporation depends on the potential evaporation, which may be considered similar every year (taking into account interannual variability), and on the water table depth, which decreased throughout the modelled period but was countered by the brine pumping (Fig. 13B). Consequently, the outflows of the system exhibit lower oscillation amplitudes than the inflows.

In the Salar de Atacama, the natural water balance was modified by the beginning of the brine exploitation. From then on, a new negative component was added to the water balance of the system. However, there is no linear relationship between the water pumped and the decrease in storage. This behaviour is associated with the damping capacity of salt flats. When a certain volume of brine is extracted, a drawdown in the water table is generated, which causes a reduction in the evaporation rate due to an increase in the thickness of the unsaturated zone. Therefore, an increase in the brine pumping rate implies a decrease in the evaporation rate, counteracting, in part, the effect of brine pumping on the total water balance (Fig. 13B). Although the drawdown of the water table may favour the influx of water from the side of the salt flat or from the depth, which are difficult to assess, the main factor responsible for the damping capacity is the modification of the evaporation rate. From an ecological point of view this damping effect may reduce the impacts of the mixing zone on lake and wetland ecosystems. However, it must be considered that the damping capacity is limited to the movement of the water table at depths shallower than 2 m. Below this depth, the evaporation rate goes to zero, and the damping capacity is lost.

The biggest contributor to the damping capacity of the salt flat water table is the nucleus, at least when the natural or anthropic disturbances are small or moderate. This is due to two reasons: (1) the large extent of the nucleus and (2) the location of the brine pumping wells. The nucleus of the salt flats generally has a large extent, which implies that even though the evaporation rate is much lower than that of the mixing zone, a small rise or fall of the water table leads to a significant change within the total water balance. This is applicable for both natural and anthropogenic disturbances. In addition, because the brines are more evaporated and therefore have a higher economic value in the salt flat nucleus, the brine pumping wells are located in that sector. Due to brine pumping, the nucleus suffers the greatest impact in terms of hydraulic heads and consequently evaporation rates.

5. Conclusions

The coupled natural and anthropogenic processes that control the hydrodynamics of many salt flats were addressed using the Salar de Atacama as a case study. A three-dimensional groundwater flow model was used to reproduce the water table evolution of the Salar de Atacama from 1986 to 2015. This also permitted quantifying the water balance impacts. The three-dimensional approach for the modelling of the groundwater flow in salt flats was demonstrated to be a power tool to evaluate natural processes and anthropogenic impacts and to be of great utility for the management of these systems.

The natural hydrodynamics of the Salar the Atacama was evidenced during the pre-operational period (1986–1994). In the natural regime, the water table exhibited a gradual drawdown because the evaporation was greater than the recharge most of the time. This negative balance was counteracted by some sharp rises produced by direct rainfall events on the salt flat. The lateral recharge that arrived from the mountains did not produce abrupt perturbations to the water table because the rainfall events in the mountains were damped by the distance from the recharge zone and the great thickness of the unsaturated zone.

The natural regime of the water table was disturbed by the brine pumping performed in the Salar de Atacama during the operational period (1994–2015). The pumping causes a fall in the water table, which results in a decrease of the evaporation rate that at least partially compensates for the pumped brine. This effect is termed in the present work the *damping capacity* of the salt flats. Due to this process, salt flats have a capacity for damping their water tables in response to both natural and anthropogenic disturbances, which is of great importance for the management of lake and wetland ecosystems and brine mining. The limit of the damping capacity of salt flats is defined by the evaporation extinction depth, which is between 0.5 and 2 m.

Acknowledgments

The authors acknowledge Sociedad Química y Minera de Chile S.A. for their support and sharing data throughout the hydrogeological characterization of the SdA site. M.A. Marazuela gratefully acknowledges the financial support from the AGAUR (Agència de Gestió d'Ajuts Universitaris i de Recerca, Generalitat de Catalunya) and the European Union (grant number 2018FI B2 00068). Finally, we thank four anonymous reviewers for their valuable comments.

Appendix A. Supplementary data

Supplementary data to this article can be found online at https://doi.org/10.1016/j.scitotenv.2018.11.196.

References

Acosta, O., Custodio, E., 2008. Impactos ambientales de las extracciones de agua subterranea en el Salar del Huasco (norte de Chile). Bol. Geol. Min. 119, 33–50.
Arriagada, C., Cobbold, P.R., Roperch, P., 2006. Salar de Atacama basin: a record of compressional tectonics in the central Andes since the mid-Cretaceous. Tectonics 25, TC1008. https://doi.org/10.1029/2004TC001770.
Bakalowicz, M., 2005. Karst groundwater: a challenge for new resources. Hydrogeol. J. 13, 148–160. https://doi.org/10.1007/s10040-004-0402-9.
Bookhagen, B., Strecker, M.R., 2008. Orographic barriers, high-resolution TRMM rainfall, and relief variations along the eastern Andes. Geophys. Res. Lett. 35, L06403. https://doi.org/10.1029/2007GL032011.
Boutt, D.F., Hynek, S.A., Munk, L.A., Corenthal, L.G., 2016. Rapid recharge of fresh water to the halite-hosted brine aquifer of Salar de Atacama, Chile. Hydrol. Process. 30, 4720–4740. https://doi.org/10.1002/hyp.10994.
Bowen, B.B., Kipnis, E.L., Raming, L.W., 2017. Temporal dynamics of flooding, evaporation, and desiccation cycles and observations of salt crust area change at the Bonneville Salt Flats, Utah. Geomorphology 299, 1–11. https://doi.org/10.1016/j.geomorph.2017.09.036.
Comisión Regional del Medio Ambiente, 2006. Resolución de Calificación Ambiental N°226/2006. Antofagasta, Chile.
Corenthal, L.G., Boutt, D.F., Hynek, S.A., Munk, L.A., 2016. Regional groundwater flow and accumulation of a massive evaporite deposit at the margin of the Chilean Altiplano. Geophys. Res. Lett. 43, 8017–8025. https://doi.org/10.1002/2016GL070076.
Cornellà, O., Salas, J., Aravena, R., Guzmán, E., Guimerà, J., Tore, C., Von Igel, W., Henríquez, A., Fock, A., 2009. Hidrogeologia de los sistemas lagunares del margen E del Salar de Atacama. XII Congreso Geológico Chileno, Santiago de Chile, pp. 1–4.
Diersch, H.-J.G., 2014. FEFLOW: finite element modeling of flow. Mass and Heat Transport in Porous and Fractured Media https://doi.org/10.1007/978-3-642-38739-5.
Doherty, J., 2015. Calibration and uncertainty analysis for complex environmental models. Groundwater 56, 673–674.
Duffy, C.J., Al-Hassan, S., 1988. Groundwater circulation in a closed desert basin: topographic scaling and climatic forcing. Water Resour. Res. 24, 1675–1688. https://doi.org/10.1029/WR024i010p01675.
Evans, R.K., 1978. Lithium reserves and resources. Energy 3, 379–385.
Fan, Y., Duffy, C.J., Oliver, D.S., 1997. Density-driven groundwater flow in closed desert basins: field investigations and numerical experiments. J. Hydrol. 196, 139–184. https://doi.org/10.1016/S0022-1694(96)03292-1.
Hamann, E., Post, V., Kohfahl, C., Prommer, H., Simmons, C.T., 2015. Numerical investigation of coupled density-driven flow and hydrogeochemical processes below playas. Water Resour. Res. 51, 9338–9352. https://doi.org/10.1002/2015WR017833.
Hardie, L.A., 1991. On the significance of evaporites. Annu. Rev. Earth Planet. Sci. 19, 131–168.
Holzbecher, E., 2005. Groundwater flow pattern in the vicinity of a salt lake. Hydrobiologia 532, 233–242.
Houston, J., 2006. Variability of precipitation in the Atacama Desert: its causes and hydrological impact. Int. J. Climatol. 26, 2181–2198. https://doi.org/10.1002/joc.1359.
IDAEA-CSIC, 2017. Cuarta actualización del modelo hidrogeológico del Salar de Atacama. Santiago, Chile.
Kampf, S.K., Tyler, S.W., 2006. Spatial characterization of land surface energy fluxes and uncertainty estimation at the Salar de Atacama, Northern Chile. Adv. Water Resour. 29, 336–354. https://doi.org/10.1016/j.advwatres.2005.02.017.
Kampf, S.K., Tyler, S.W., Ortiz, C.A., Muñoz, J.F., Adkins, P.L., 2005. Evaporation and land surface energy budget at the Salar de Atacama, Northern Chile. J. Hydrol. 310, 236–252. https://doi.org/10.1016/j.jhydrol.2005.01.005.

Karl, T.R., Williams, C.N., 1987. An approach to adjusting climatological time series for discontinuous inhomogeneities. J. Clim. Appl. Meteorol. 26, 1744–1762. https://doi.org/10.1175/1520-0450(1987)026<1744:AATACT>2.0.CO;2.

Kesler, S.E., Gruber, P.W., Medina, P.A., Keoleian, G.A., Everson, M.P., Wallington, T.J., 2012. Global lithium resources: relative importance of pegmatite, brine and other deposits. Ore Geol. Rev. 48, 55–69. https://doi.org/10.1016/j.oregeorev.2012.05.006.

Lowenstein, T.K., Risacher, F., 2009. Closed basin brine evolution and the influence of Ca-Cl inflow waters: Death Valley and Bristol Dry Lake California, Qaidam Basin, China, and Salar de Atacama, Chile. Aquat. Geochem. 15, 71–94. https://doi.org/10.1007/s10498-008-9046-z.

Marazuela, M.A., Vázquez-Suñé, E., Custodio, E., Palma, T., García-Gil, A., Ayora, C., 2018. 3D mapping, hydrodynamics and modelling of the freshwater-brine mixing zone in salt flats similar to the Salar de Atacama (Chile). J. Hydrol. 561, 223–235. https://doi.org/10.1016/j.jhydrol.2018.04.010.

Marazuela, M.A., Vázquez-Suñé, E., Ayora, C., García-Gil, A., Palma, T., 2019. Hydrodynamics of salt flat basins: the Salar de Atacama example. Sci. Total Environ. 651, 668–683. https://doi.org/10.1016/j.scitotenv.2018.09.190.

Marom, R., Amalraj, S.F., Leifer, N., Jacob, D., Aurbach, D., 2011. A review of advanced and practical lithium battery materials. J. Mater. Chem. 21, 9938–9954. https://doi.org/10.1039/c0jm04225k.

Mpodozis, C., Arriagada, C., Basso, M., Roperch, P., Cobbold, P., Reich, M., 2005. Late Mesozoic to Paleogene stratigraphy of the Salar de Atacama Basin, Antofagasta, Northern Chile: implications for the tectonic evolution of the Central Andes. Tectonophysics 399, 125–154. https://doi.org/10.1016/j.tecto.2004.12.019.

Munk, L.A., Hynek, S.A., Bradley, D., Boutt, D.F., Labay, K., Jochens, H., 2016. Lithium brines: a global perspective. Rev. Econ. Geol. 18, 339–365.

Muñoz, N., Charrier, R., Jordan, T., 2002. Interactions between basement and cover during the evolution of the Salar de Atacama Basin, northern Chile. Rev. Geol. Chile 29, 3–29. https://doi.org/10.4067/S0716-02082002000100004.

Muñoz-Pardo, J.F., Ortiz-Astete, C.A., Mardones-Pérez, L., de Vidts-Sabelle, P., 2004. Funcionamiento hidrogeológico del acuífero del núcleo del salar de Atacama, Chile. Ing. Hidráulica en Mex XIX, 69–81.

Nield, D.A., Simmons, C.T., Kuznetsov, A.V., Ward, J.D., 2008. On the evolution of salt lakes: episodic convection beneath an evaporating salt lake. Water Resour. Res. 44, W02439. https://doi.org/10.1029/2007WR006161.

Ortiz, C., Aravena, R., Briones, E., Suárez, F., Tore, C., Muñoz, J.F., 2014. Sources of surface water for the Soncor ecosystem, Salar de Atacama basin, northern Chile. Hydrol. Sci. J. 59, 336–350. https://doi.org/10.1080/02626667.2013.829231.

Pananont, P., Mpodozis, C., Blanco, N., Jordan, T.E., Brown, L.D., 2004. Cenozoic evolution of the northwestern Salar de Atacama Basin, northern Chile. Tectonics 23, 1–19. https://doi.org/10.1029/2003TC001595.

Peterson, T.C., Easterling, D.R., 1994. Creation of homogeneous composite climatological reference series. Int. J. Climatol. 14, 671–679. https://doi.org/10.1002/joc.3370140606.

Philip, J.R., 1957. Evaporation, and moisture and heat fields in the soil. J. Meteorol. 14, 354–366. https://doi.org/10.1175/1520-0469(1957)014<0354:EAMAHF>2.0.CO;2.

Rech, J.A., Currie, B.S., Michalski, G., Cowan, A.M., 2006. Neogene climate change and uplift in the Atacama Desert, Chile. Geology https://doi.org/10.1130/G22444.1.

Risacher, F., Alonso, H., Salazar, C., 2003. The origin of brines and salts in Chilean salars: a hydrochemical review. Earth Sci. Rev. 63, 249–293. https://doi.org/10.1016/S0012-8252(03)00037-0.

Rissmann, C., Leybourne, M., Benn, C., Christenson, B., 2015. The origin of solutes within the groundwaters of a high Andean aquifer. Chem. Geol. 396, 164–181. https://doi.org/10.1016/j.chemgeo.2014.11.029.

Rockwood-Lithium, 2015. Estudio Hidrogeológico y Modelo Numérico Sector Sur del Salar de Atacama (Anexo 1). Para Estudio de Impacto Ambiental Proyecto Modificaciones y Mejoramiento del Sistema de Pozas de Evaporación solar en el Salar de Atacama. Santiago, Chile.

Rosen, M.R., 1994. The importance of groundwater in playas: a review of playa classifications and the sedimentology and hydrology of playas. Geol. Soc. Am. Spec. Pap. 289, 1–18. https://doi.org/10.1130/SPE289-p1.

Salas, J., Guimerà, J., Cornellà, O., Aravena, R., Guzmán, E., Tore, C., Von Igel, W., Moreno, R., 2010. Hidrogeologia del sistema lagunar del margen este del Salar de Atacama (Chile). Bol. Geol. Min. 121, 357–372.

Scanlon, B.R., Mace, R.E., Barrett, M.E., Smith, B., 2003. Can we simulate regional groundwater flow in a karst system using equivalent porous media models? Case study, Barton Springs Edwards aquifer, USA. J. Hydrol. 276, 137–158. https://doi.org/10.1016/S0022-1694(03)00064-7.

Tejeda, I., Cienfuegos, R., Muñoz, J.F., Durán, M., 2003. Numerical modeling of saline intrusion in Salar de Atacama. J. Hydrol. Eng. 8, 25–34. https://doi.org/10.1061/(ASCE)1084-0699(2003)8:1(25).

Tyler, S.W., Muñoz, J.F., Wood, W.W., 2006. The response of playa and Sabkha hydraulics and mineralogy to climate forcing. Ground Water 44, 329–338. https://doi.org/10.1111/j.1745-6584.2005.00096.x.

Vásquez, C., Ortiz, C., Suárez, F., Muñoz, J.F., 2013. Modeling flow and reactive transport to explain mineral zoning in the Atacama salt flat aquifer, Chile. J. Hydrol. 490, 114–125. https://doi.org/10.1016/j.jhydrol.2013.03.028.

Vikström, H., Davidsson, S., Höök, M., 2013. Lithium availability and future production outlooks. Appl. Energy 110, 252–266. https://doi.org/10.1016/j.apenergy.2013.04.005.

Warren, J.K., 2010. Evaporites through time: tectonic, climatic and eustatic controls in marine and nonmarine deposits. Earth Sci. Rev. 98, 217–268. https://doi.org/10.1016/j.earscirev.2009.11.004.

Wood, W.W., Sanford, W.E., 1990. Ground-water control of evaporite deposition. Econ. Geol. 85, 1226–1235. https://doi.org/10.2113/gsecongeo.85.6.1226.

Wooding, R.A., Tyler, S.W., White, I., 1997. Convection in groundwater below an evaporating Salt Lake: 1. Onset of instability. Water Resour. Res. 33, 1199–1217. https://doi.org/10.1029/96WR03533.

Yechieli, Y., Wood, W.W., 2002. Hydrogeologic processes in saline systems: playas, sabkhas, and saline lakes. Earth Sci. Rev. 58, 343–365. https://doi.org/10.1016/S0012-8252(02)00067-3.